JOURNAL OF PROPULSION AND POWER
Vol. 19, No. 1, January–February 2003

Bypass-Regulated Solid Fuel Ramjet Combustor in Variable Flight Conditions

Deborah Pelosi-Pinhas* and Alon Gany†
Technion—Israel Institute of Technology, 32000 Haifa, Israel

A comprehensive experimental investigation aimed at the examination of a solid fuel ramjet (SFRJ) regulation concept using an air-division valve has been conducted. By controlling the ratio between the port and bypass flows, one can maintain a desirable working state over a wide range of flight conditions. A general regulation law based on maintaining a constant fuel-to-air ratio has been tested. The experimental strategy was to isolate key parameters influencing the fuel regression rate, testing them one at a time, keeping the other parameters constant. Experiments aimed at airflow rate, total air temperature and pressure, as well as port diameter effects, simulated a broad flight envelope, from Mach 1.5 to Mach 4.7 and from sea level to 13-km altitude. The test results showed a very good agreement with the theory, demonstrating the feasibility, effectiveness, and characteristics of the air-division valve regulation technique in SFRJ motors.

Nomenclature

A	=	cross-sectional area
a	=	burning rate constant
C	=	constant
d	=	diameter
f	=	fuel-to-air ratio
M	=	Mach number
m	=	total temperature exponent
$\dot{m}$	=	mass flow rate
n	=	mass flow rate exponent
P	=	pressure
q	=	port diameter exponent
$\dot{r}$	=	fuel regression rate
s	=	port-to-inlet diameter ratio exponent
T	=	temperature

Subscripts

a	=	air
b	=	bypass
c	=	combustion
f	=	fuel
in	=	inlet
nom	=	nominal
p	=	port
t	=	throat
0	=	stagnation (total) conditions

Introduction

THE objective of the present work was to conduct a comprehensive experimental investigation to examine and provide actual characteristics of a concept for the regulation of solid fuel ramjet (SFRJ) combustor for optimal operation over a broad range of variable conditions. This concept was presented and analyzed theoretically by Pelosi-Pinhas and Gany[1] and seemed to offer good control capabilities. The method is based on the use of an air-division valve, which divides the incoming airflow from the diffuser into two separate flows (Fig. 1): A part of the air (the port or principal airflow) is drawn directly into the combustion chamber through the port of the solid fuel, influencing the fuel regression rate, while the other part (the bypass airflow) flows through a bypass to the aft-mixing section of the combustion chamber, determining the overall fuel-to-air ratio.

The analytical study was aimed at formulating a general regulation law for the air-division valve in terms of the instantaneous proportion between the port and bypass flow rates. The current experimental investigation demonstrates the actual behavior via static firing tests simulating a broad range of flight and ambient conditions.

Ramjet engines may be considered for long-range missile propulsion because their energetic performance is superior to that of rocket motors (demonstrated by their three- to five-fold higher specific impulse). Among the different ramjet configurations, the SFRJ provides particular simplicity and safety, as well as high specific impulse.[2,3]

One of the disadvantages of the SFRJ motor is the uncontrollability of its combustion process, where key operating parameters, such as the fuel regression rate and the fuel-to-air ratio, are affected by flight and ambient conditions. This is a result of the dominating properties (mainly Reynolds number and stagnation temperature) of the incoming air flowing through the port of the solid fuel grain. Hence, operation over variable conditions of flight altitudes and Mach numbers may result in large deviations from the desired combustor working point, lower performance, and, under extreme conditions, even motor extinction.

The concept of bypass regulation for SFRJ motors is discussed by Leisch and Netzer.[4] Krishnan and George[5] and Krishnan et al.[6] conducted theoretical studies examining a specific version of the regulation technique for a typical configuration of SFRJ gun-launched projectiles. The fuel regression rate control method used in their numerical work consisted of the so-called tube-in-hole concept,[7] in which a tube coaxially placed in the grain port is used to divide the inlet air mass flow rate, so that only the desired quantity of air influences the fuel combustion rate.

Obviously, there is a lack of experimental examination of the SFRJ regulation concept in the professional literature. A brief reference to the analytical work of Pelosi-Pinhas and Gany[1] and to the resulting regulation law will be made, followed by a detailed presentation of the experimental study.

Analysis

The incoming air to the SFRJ combustor is assumed to flow through a cylindrical single port within the fuel grain placed in the combustion chamber.

Received 31 August 2001; revision received 22 July 2002; accepted for publication 13 September 2002.

*Ph.D. Student, Faculty of Aerospace Engineering; debby@aerodyne.technion.ac.il.

†Professor, Lena and Ben Fohrman Chair in Aeronautical Engineering, Head, Fine Rocket Propulsion Center, Faculty of Aerospace Engineering; gany@aerodyne.technion.ac.il. Associate Fellow AIAA.

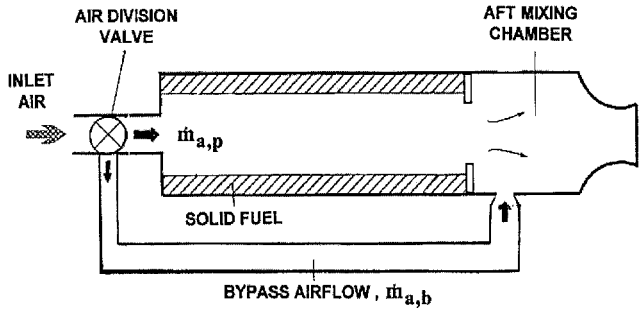

Fig. 1 Schematic of the combustion chamber showing the air-division valve concept.

The fuel regression rate model presented by Hadar and Gany[8] has been used, taking into consideration the parameters influencing the combustion process and using physical approximations. The model assumes the existence of a diffusion flame over the condensed fuel surface, dominated by a forced convective heat transfer mechanism through the turbulent boundary layer. Making use of Reynolds analogy in a developed turbulent boundary layer and assuming constant gas properties, the fuel regression rate may be expressed in terms of the port air mass flow rate and the port diameter as follows:

$$\dot{r} \propto \dot{m}_{a,p}^{n} d^{-(1+n)} \tag{1}$$

From the experience of previous works, the dominant effect of total air temperature on fuel regression rate can be incorporated in terms of an exponential influence:

$$\dot{r} \propto \dot{m}_{a,p}^{n} d^{-(1+n)} T_0^{m} \tag{2}$$

The total temperature exponent m is determined experimentally similarly to the mass flow rate exponent n. This model gives a general scheme, which can be replaced or improved by test data or other available correlations.

The air-division valve concept is based on fuel regression rate regulation capability via port airflow control, whereas the overall fuel-to-air ratio depends on the overall air mass flow rate, which includes both port and bypass airflows:

$$f = \dot{m}_f / \dot{m}_a = \dot{m}_f / (\dot{m}_{a,p} + \dot{m}_{a,b}) \tag{3}$$

Making use of Eq. (2), one can express the fuel mass flow rate as a function of the port air mass flow rate, the port diameter, and the total air temperature:

$$\dot{m}_f \propto (\dot{m}_{a,p}/d)^{n} \cdot T_0^{m} \tag{4}$$

In this study, the regulation requirement is defined as the motor capability of operating at a constant, desirable fuel-to-air ratio. Nominal conditions are defined, at which a nominal value of fuel burning rate and a desirable nominal value of fuel-to-air ratio occur. When the fuel-to-air ratio at any point in the flight envelope is compared to the desired nominal one, a general control law is derived, defining the instantaneous opening state of the air-division valve represented by the port-to-total air mass flow rates ratio as a function of air mass flow rate, air stagnation temperature, and port diameter, relative to the nominal conditions

$$\dot{m}_{a,p}/\dot{m}_a = (\dot{m}_{a,p}/\dot{m}_a)_{\text{nom}} \cdot (d/d_{\text{nom}}) \cdot (\dot{m}_a/\dot{m}_{a,\text{nom}})^{[(1-n)/n]} \cdot (T_0/T_{0,\text{nom}})^{-(m/n)} \tag{5}$$

The nominal port-to-total air mass flow rates ratio is calculated by taking into account the most extreme conditions over the operating envelope, where the entire amount of the air should flow through the port.

When use is made of the regulation law in Eq. (5) and the regression rate model of Eq. (2), the burning rate can be predicted in terms of the instantaneous opening state of the valve, the air mass flow rate, total air temperature, and port diameter, by relating it to the nominal conditions:

$$\dot{r} = \dot{r}_{\text{nom}} \cdot (\dot{m}_{a,p}/\dot{m}_a)^{n} \Big/ (\dot{m}_{a,p}/\dot{m}_a)_{\text{nom}}^{n} \cdot (\dot{m}_a/\dot{m}_{a,\text{nom}})^{n} \cdot (d/d_{\text{nom}})^{-(1+n)} \cdot (T_0/T_{0,\text{nom}})^{m} \tag{6}$$

It is possible to express the control law in a more general form as a function of flight conditions, by defining air mass flow rate and total air temperature in terms of flight altitude and Mach number.[1]

Based on the theoretical analysis, Pelosi-Pinhas and Gany[1] applied the control law to a theoretical simulation of some practical examples. The port-to-total air mass flow rates ratio ($\dot{m}_{a,p}/\dot{m}_a$), representing the opening state of the air-division valve, has been determined as a function of time for two representative trajectories: linear climbing from sea level to 15 km and linear descent from 15 km to sea level, both at a constant flight Mach number ($M = 2.5$). A parametric analysis was conducted, based on the variation of influencing parameters, such as initial fuel port diameter and fuel regression rate characteristic exponents m and n. The numerical investigation demonstrated that theoretically the opening state of the valve can be successfully determined at any operating point during flight. Conceptually, the air-division valve regulation seems to offer good control capabilities, enabling optimal motor operation at a desirable constant fuel-to-air ratio over a wide operating range. In practice, aspects of the combustor behavior, such as flameholding and the actual characteristics of fuel combustion, remained to be determined experimentally.

Experimental Apparatus

General

The experimental apparatus is shown schematically in Fig. 2 and a photograph of the facility is shown in Fig. 3. The test facility includes a vitiated air heater, an ignition system, a combustion chamber, an

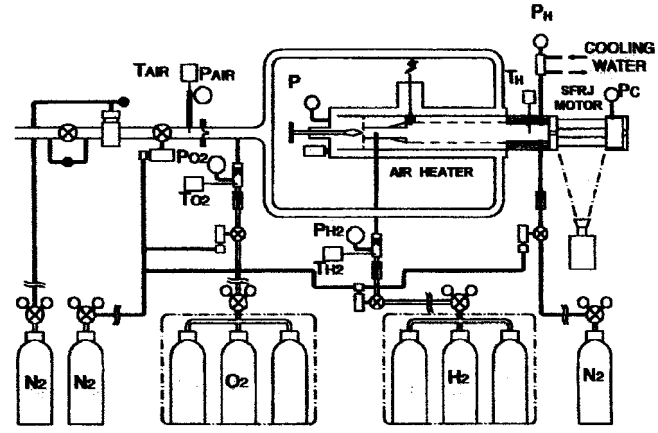

Fig. 2 Elaborated scheme of the experimental apparatus.

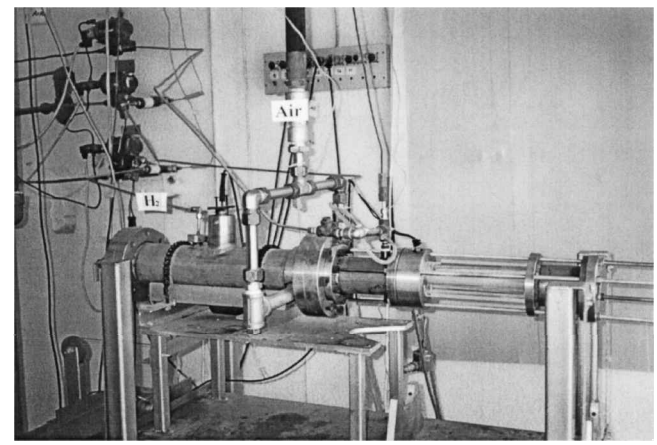

Fig. 3 General view of the experimental facility.

aft-mixing chamber, and a motor outlet nozzle. The regeneratively cooled vitiated air heater[9] is used to simulate flight conditions, defined by total temperature and pressure of the air mass flow rate entering the combustion chamber. The heater can provide vitiated air to the combustion chamber at inlet total temperatures up to 1500 K, pressures up to 50 atm, and mass flow rates as high as 1000 g/s. In the present study, air total temperature varied from 395 to 1200 K, total pressure reached up to 20 atm, and air mass flow rates were between 50 and 270 g/s. The vitiated air heater burns hydrogen with oxygen-enriched air to reach the desired total inlet air temperature. Compressed air, hydrogen, and oxygen are provided to the heater from high-pressure tanks. Their required mass flow rates are determined by using a thermodynamic code (PEP code[10]) to obtain the molar oxygen fraction of the vitiated air as in natural air (0.209).

Poly-methyl-methacrylate(PMMA-Plexiglas®) was used as fuel, serving also as the combustor itself. The transparency and the mechanical strength of Plexiglas make it particularly suitable for experimental investigations because it enables instantaneous observation of the flow and the combustion phenomena without any need for outer casing.

The design of the combustion chamber (inlet step, fuel port area, and outlet nozzle throat area) takes into consideration the flameholding limits of PMMA, according to precedent work.[11] The air enters the combustion chamber through a 10-mm inlet diameter passage, and the initial fuel port diameter is 20 mm, yielding an inlet step height of 5 mm, or in terms of the port-to-inlet area ratio, $A_p/A_{\text{in}} = 4$. The outlet nozzle throat diameter varied from 7.5 to 17 mm, providing the desired chamber pressure and a port-to-nozzle throat area ratio $A_p/A_t = 1.4$–7.1. These conditions ensured flameholding in the desired working temperature range. Final internal diameter of 40–50 mm at combustor burnout could be reached considering the Plexiglas thickness necessary to withstand the chamber pressure. The fuel grain length was 240 mm, and the aft-mixing chamber length was 100 mm.

Each test consisted of an automatically relayed 10–15 s preheat phase, needed to raise air temperature to the desired value at the heater outlet, followed by a manually controlled ignition command and a short burning phase (4–5 s) of the solid fuel. Four sets of experiments have been performed, enabling characterization of fuel regression rate as a function of the major influencing parameters.

Ignition

In most of the cases, the operating range of total air temperatures did not enable self-ignition of the PMMA fuel; hence, an ignition device was designed, fabricated, and integrated to the experimental facility between the heater and the combustion chamber. The device consists of three elements: the igniter chamber incorporated within the combustor head-end assembly, a small cylindrical solid propellant grain, and a sealing plug closing the igniter case. The propellant ignites by means of an electrically heated wire actuated by a computer-relayed command. The hot igniter gases are released into the flow recirculation zone within the combustion chamber through a passage in the inlet step, resulting in fuel surface fast heating and ignition. To increase the hot gases release duration, most of the igniter propellant's surface is covered with epoxy to produce a slower and almost neutral burning rate along its axis.

Data Acquisition and Control

A computer-relayed automatic system is used to perform both the experimental sequence of commands and the acquisition of data. The same software is used to handle both the automated control system via a digital I/O board and data acquisition via an A/D board.

The test facility comprises several measurement points: temperature and pressure at the heater exit, combustor pressure measurement, placed in the aft-mixing chamber, and a thrust measurement. In addition, the mass flow rates of the air, hydrogen, and oxygen are measured and regulated by using sonic nozzles with upstream pressure and temperature measurements.

A video camera is used in all experiments to record the solid fuel regression history, allowing instantaneous geometrical measurements and fuel mass flow rate calculation.

Results

General

Experimental examination of the regulation concept via static tests is complex because of the many different parameters affecting the combustion process. To not obscure the picture by a multitude of simultaneous variation of different influencing parameters, and to perform a careful and efficient study, the experimental strategy was based on the isolation of the key parameters, varying a single operating parameter at a time, keeping the remaining operating conditions more or less constant. Air mass flow rate, inlet air total temperature, chamb pressure, as well as port diameter were considered separately, formulating the control law specific to each case and comparing test results to the theoretical predictions. A total of 30 tests were performed.

The air-division valve concept is based on the port conditions' effect on fuel mass flow rate, regulating the fuel regression rate to meet the requirement of motor operation at constant overall fuel-to-air ratio according to the control law. Hence, the static test apparatus does not require an actual air-division valve and bypass systems because the control is performed essentially via the port air mass flow rate variation.

Four sets of experiments were conducted, where each set isolates a different influencing parameter keeping the others constant. The experimental results as well as their accuracy are shown in Table 1. The accuracy of the calculated parameters result from a composite sensitivity calculation considering all influences, whereas measured parameters' accuracy is determined independently. The air

Table 1 Results of the four experimental sets[a]

Test no.	d_{av},[b] mm	$\dot{m}_{a,p}$,[b] g/s	$T_{0,\text{in}}$,[c] K	P_c,[d] atm	$\dot{m}_f$,[e] g/s	f_{port}[e]	$\dot{r}$,[c] mm/s
			Set 1				
1	21.6	**48.3**	830	5.6	7.5	0.155	0.421
2	23.4	**70.6**	840	8.1	10.16	0.144	0.481
3	24.1	**96.2**	847	11.2	12.1	0.126	0.555
4	24.2	**144.7**	873	12.6	18.96	0.13	0.86
5	25.5	**166.2**	847	19.9	20.7	0.124	0.897
6	26.2	**190.6**	849	17.7	24.1	0.127	1.02
7	26.2	**212.1**	880	12.1	26.0	0.122	1.097
8	26.3	**242.7**	863	14.6	29.8	0.123	1.248
9	26.9	**262.1**	863	19.4	32.73	0.1248	1.345
			Set 2				
10	22.8	67.7	**562**	7.2	5.47	0.08	0.265
11	22.0	68.4	**632**	7.4	7.12	0.104	0.342
12	22.5	68.3	**811**	7.8	8.9	0.13	0.443
13	23.4	70.6	**840**	7.6	10.16	0.144	0.481
14	23.2	66.5	**865**	7.7	10.87	0.163	0.496
15	23.4	68.1	**1000**	8.1	11.23	0.165	0.53
16	24.2	68.6	**1100**	8.6	12.26	0.178	0.560
17	24.0	68.6	**1200**	8.8	14.2	0.207	0.621
			Set 3				
18	**32.3**	96.4	904	11.4	15.4	0.16	0.527
19	**39.5**	96.6	800	11.1	17.8	0.185	0.499
20	**45.5**	96.8	813	11.2	18.5	0.191	0.449
21	**23.2**	164.2	864	13.2	19.8	0.120	0.873
21	**32.4**	165.6	395	11.8	22.2	0.134	0.757
22	**39.0**	165.5	850	13.2	20.7	0.125	0.542
23	**43.5**	165.5	395	11.9	14.63	0.088	0.372
24	**39.6**	260.4	863	18.9	31.6	0.121	0.88
25	**50.2**	262.8	863	17.1	35.7	0.135	0.787
26	**25.4**	69.5	799	7.9	10.1	0.145	0.44
27	**35.6**	69.5	807	7.9	12.14	0.174	0.377
28	**41.8**	69.7	801	7.8	13.07	0.187	0.346
			Set 4				
29	22.9	59.5	867	**3.4**	8.66	0.146	0.422
30	23.0	59.4	867	**8.9**	9.13	0.153	0.438
31	22.7	59.4	867	**15.9**	8.66	0.146	0.445

[a]Varying parameter in each set in bold face.
[b]Accuracy of 2%.
[c]Accuracy of 10%.
[d]Accuracy of 1%.
[e]Accuracy of 6%.

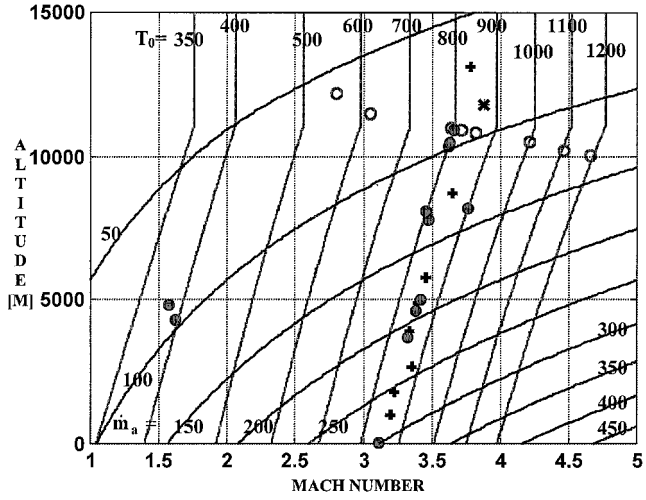

+ Port mass flow rate variation tests

o Air total temperature variation tests

● Port diameter variation tests

⋆ Chamber pressure variation test

Fig. 4 The simulated flight envelope showing constant air mass flow rate lines (grams per second), constant total air temperature lines (degrees Kelvin), and experimental points.

mass flow rate and air total temperature ranges are shown in Fig. 4, presenting the equivalent simulated flight points in the experimental study over a map of flight conditions. Nominal conditions were sea level, air total temperature of 807 K (simulating Mach 3 flight at sea level), and average port diameter of 23 mm. Air total temperature varied from 395 to 1200 K, and port air mass flow rates were between 50 and 270 g/s. The nominal overall air mass flow rate was 300 g/s. Chamber pressure varied from 0.6 to 2 MPa. The experimental results simulated a wide envelope of operating altitudes (0–13 km) and Mach numbers (1.5–4.7).

Air Mass Flow Rate Variation

A first series of tests investigated the air mass flow rate influence on fuel regression rate with approximately constant total inlet temperature and average port diameter, enabling fuel regression rate characterization by identifying the actual n exponent in the regression rate correlation. Experimental results yielded a basic correlation of fuel regression rate as a function of port air mass flow rate at the nominal port diameter and a total air temperature of 850 K:

$$\dot{r} = 0.0153 \times \dot{m}_{a,p}^{0.8} \tag{7}$$

where $\dot{r}$ is in millimeters per second and $\dot{m}$ is in grams per second. Figure 5 shows both the experimental results and the correlation with $n = 0.8$ as a function of the air mass flow rate. The $n = 0.8$ exponent of the air mass flow rate is consistent with turbulent boundary-layer theory.[12]

Once fuel regression rate is characterized, one can make use of the control law and compare the experimental results to the theoretical prediction. For the experimental simulation, the nominal operating conditions are defined as follows: $(\dot{m}_a)_{\text{nom}}$ is the highest air mass flow rate, where all of the incoming air is channeled through the port, namely, $(\dot{m}_{a,p})_{\text{nom}} = (\dot{m}_a)_{\text{nom}}$. The constant port diameter is equal to the nominal diameter, namely, $d = d_{\text{nom}} = \text{const}$. One can, thus, specify and relate the operating and nominal conditions as follows:

$$f/f_{\text{nom}} = \text{const} = 1, \qquad (\dot{m}_{a,p}/\dot{m}_a)_{\text{nom}} = 1$$

$$d/d_{\text{nom}} = \text{const} = 1, \qquad T_0/T_{0,\text{nom}} = \text{const} = 1 \tag{8}$$

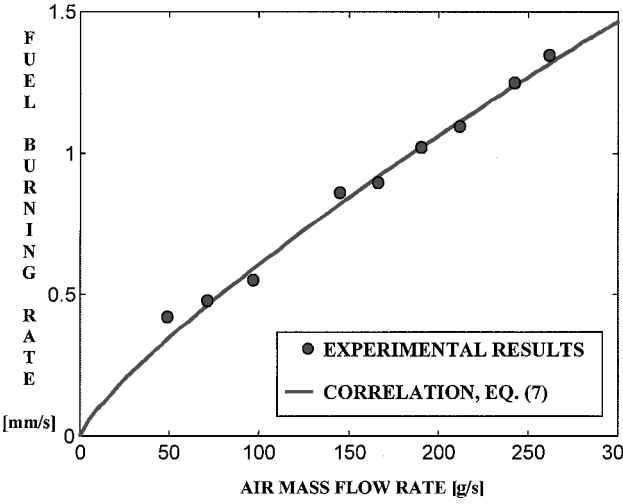

Fig. 5 Solid fuel burning rate as a function of the air mass flow rate through the port, for a constant total air temperature of 850 K and constant port diameter of 23 mm.

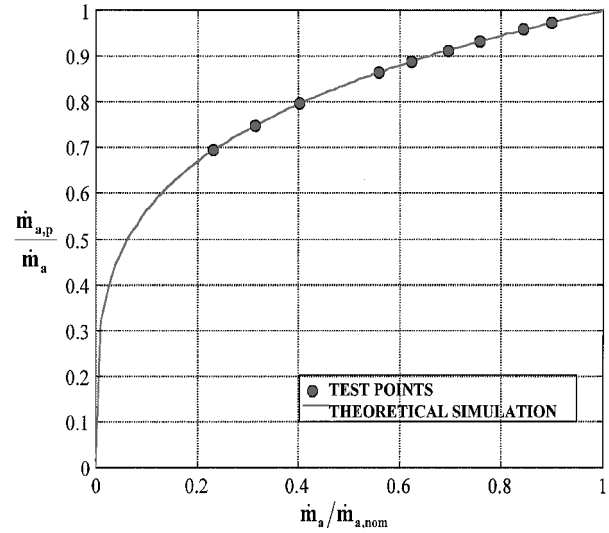

Fig. 6 Correlation of the experimental points to theoretical opening states of the air-division valve as function of normalized overall air mass flow rate, in the case of port air mass flow rate variation with constant air temperature and port diameter.

When Eq. (8) is substituted in Eq. (5), the following simplified regulation law is, thus, implied:

$$\dot{m}_{a,p}/\dot{m}_a = (\dot{m}_a/\dot{m}_{a,\text{nom}})^{(1-n)/n} \tag{9}$$

To check the control law, the experimental results need to fit some hypothetical cases, where the known port air mass flow rate from the experiments represents only a part of the total air mass flow rate in the motor. Equation (9) enables fitting each experimental case to the appropriate theoretical opening state of the valve. The function of the predicted opening state of the air-division valve and the actual simulated points are shown in Fig. 6.

By substituting Eq. (8) in Eq. (6), one can also simplify the normalized regression rate expression:

$$\dot{r}/\dot{r}_{\text{nom}} = (\dot{m}_{a,p}/\dot{m}_{a,\text{nom}})^n = \dot{m}_a/\dot{m}_{a,\text{nom}} \tag{10}$$

Figure 7 shows the regression rate line from Eq. (10) and the experimental regression rate as a function of the normalized port air mass flow rate. The predicted theoretical normalized regression rate expression results from the general control law; hence, the agreement between theoretical and experimental results is logically expected.

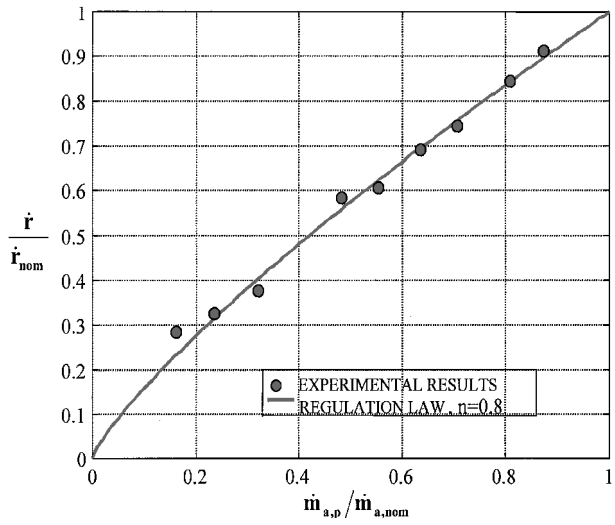

Fig. 7 Normalized burning rate (experimental and theoretical) as a function of normalized port air mass flow rate, in the case of port air mass flow rate variation with constant air temperature and port diameter.

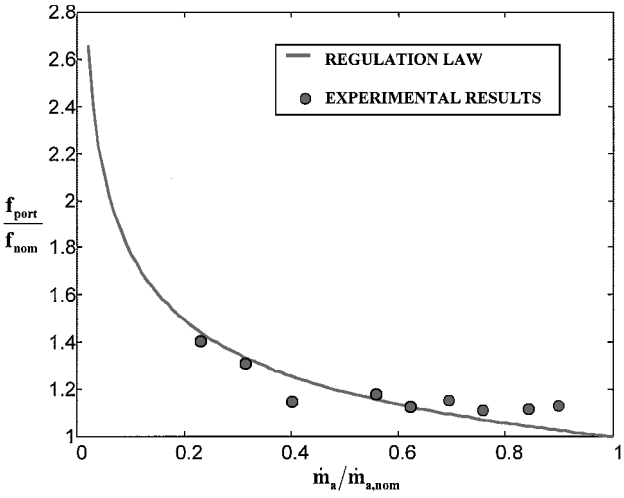

Fig. 8 Port to nominal fuel/air ratio as a function of normalized overall air mass flow rate in the case of port air mass flow rate variation with constant air temperature and port diameter.

Whereas the overall fuel-to-air ratio f remains constant and equal to the nominal fuel-to-air ratio f_{nom}, the port fuel-to-air ratio (related to the port flow only) f_p varies with the airflow rate according to

$$f_p/f = f_p/f_{\text{nom}} = (\dot{m}_{a,p}/\dot{m}_a)^{-1} = (\dot{m}_a/\dot{m}_{a,\text{nom}})^{(n-1)/n}$$
$$= (\dot{m}_{a,p}/\dot{m}_{a,\text{nom}})^{n-1} \tag{11}$$

The experimental data as well as the theoretical line of the port-to-nominal fuel-to-air ratio f_p/f_{nom} as a function of the port-to-total air mass flow rates ratio $\dot{m}_{a,p}/\dot{m}_a$ are presented in Fig. 8. The experimental results reveal a good agreement with the theoretical prediction.

Air Total Temperature Variation

The second set of experiments characterized the inlet air total temperature influence on fuel regression rate, with approximately constant port air mass flow rate and average port diameter. The experimental results yielded a correlation of fuel regression rate as a function of inlet air total temperature, where the dependence was found to be approximately linear ($m \cong 1$):

$$\dot{r} = 5.3 \times 10^{-4} \cdot T_0^1 \tag{12}$$

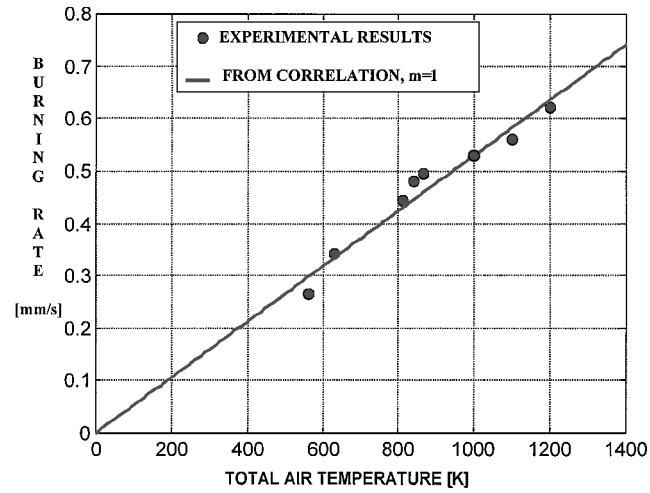

Fig. 9 Solid fuel burning rate as a function of the total temperature of the air entering the combustion chamber, for constant port airflow rate (70 g/s) and port diameter (23 mm).

where $\dot{r}$ is in millimeters per second and T_0 in is in degrees Kelvin. Figure 9 shows both the experimental results and the correlated curve as a function of total air temperature.

Similar to the air mass flow rate variation case, air total temperature variation tests were performed according to the basic requirement of constant total fuel-to-air ratio, equal to the nominal desired fuel-to-air ratio, that is, $f = f_{\text{nom}} = \text{const}$. It was also assumed that in the nominal case the total quantity of air enters the fuel port and that in these conditions the air mass flow rate is the maximal air mass flow rate entering the diffuser. Port diameter was kept approximately constant and equal to the nominal port diameter, namely, $d = d_{\text{nom}} = 23$ mm. Contrary to the former case, port air mass flow rate was constant ($\dot{m}_{a,p} = 70$ g/s), while total air temperature was varied from 550 to 1200 K, then

$$\dot{m}_{a,p}/\dot{m}_{a,\text{nom}} = \text{const} = C \tag{13}$$

Substitution of the conditions specific to the current case yields the formulation of a simplified control law for the air-division valve:

$$\dot{m}_{a,p}/\dot{m}_a = (\dot{m}_a/\dot{m}_{a,\text{nom}})^{(1-n)/n} \cdot (T_0/T_{0,\text{nom}})^{-m/n} \tag{14}$$

Making use of Eq. (13), one can express the port-to-total air mass flow rates ratio as a function of the normalized air mass flow rate and of the constant C:

$$\dot{m}_{a,p}/\dot{m}_a = \dot{m}_{a,p}/\dot{m}_{a,\text{nom}} \cdot \dot{m}_{a,\text{nom}}/\dot{m}_a = C \cdot (\dot{m}_a/\dot{m}_{a,\text{nom}})^{-1} \tag{15}$$

Substitution of Eq. (15) in Eq. (14) leads to a useful relation between the normalized air mass flow rate and the normalized total temperature:

$$(T_0/T_{0,\text{nom}})^m = C^{-n} \cdot (\dot{m}_a/\dot{m}_{a,\text{nom}}) \tag{16}$$

This expression enables relating experimental results, characterized by the knowledge of total air temperature, to the respective (hypothetical) opening states of the valve:

$$\dot{m}_{a,p}/\dot{m}_a = C^{(1-n)} \cdot (T_0/T_{0,\text{nom}})^{-m} \tag{17}$$

Figure 10 shows the opening states of the valve simulated in the experimental study according to Eqs. (16) and (17). Note that, in the specific experimental point of the lowest normalized air mass flow rate, the constant fuel-to-air requirement is not achievable because it requires a higher port air mass flow rate than is possibly available. In this extreme case, regulation is incomplete, and one should expect motor operation at a fuel-to-air ratio slightly different from the desired one, performed in the totally open valve operation state.

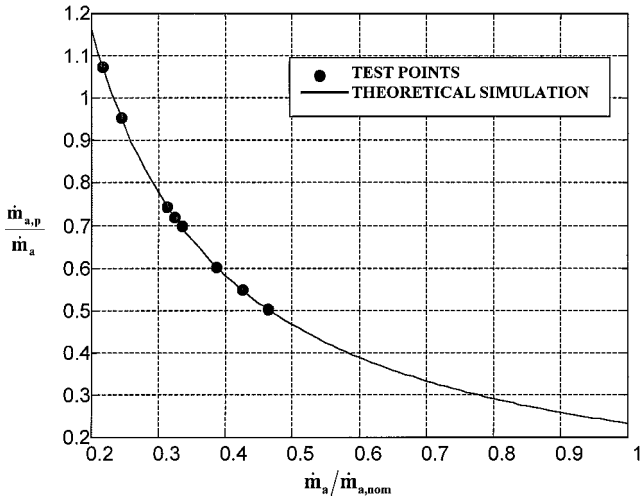

Fig. 10 Correlation of the experimental points to hypothetical opening states of the air-division valve as a function of normalized overall air mass flow rate, in the case of total air temperature variation and constant port diameter.

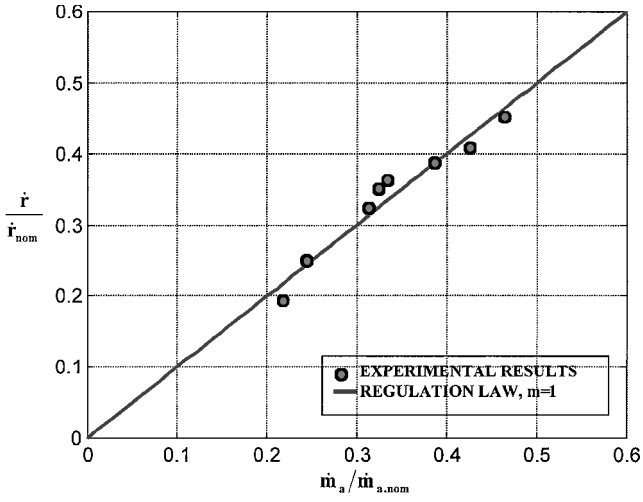

Fig. 11 Normalized fuel regression rate (experimental and theoretical) as a function of normalized overall air mass flow rate, in the case of total air temperature variation, with constant port air mass flow rate and port diameter.

Substituting the specific conditions of the total temperature variation case in Eq. (6) yields the simplified normalized regression rate expression:

$$\dot{r}/\dot{r}_{\text{nom}} = (\dot{m}_{a,p}/\dot{m}_{a,\text{nom}})^n \cdot (T_0/T_{0,\text{nom}})^m \tag{18}$$

Figure 11 presents the theoretical [Eq. (18)] and the experimental normalized regression rates, again showing predictable agreement.

The port-to-nominal fuel-to-air ratio was formulated for the current case making use of Eq. (15):

$$f_p/f_{\text{nom}} = (\dot{m}_{a,p}/\dot{m}_a)^{-1} = C^{-1} \cdot \dot{m}_a/\dot{m}_{a,\text{nom}} \tag{19}$$

The experimental and the theoretically predicted port-to-nominal fuel-to-air ratio were compared in Fig. 12, revealing good agreement and, hence, demonstrating once again the effectiveness of the air-division valve regulation concept.

Chamber Pressure Variation

The formulated model of fuel regression rate takes into account different influencing parameters, for example, air mass flow rate, air total temperature, and port diameter, without considering the chamber pressure. The work assumed that pressure effect on fuel regression rate is negligible, according to precedent works where chamber pressure has been shown to have practically no influence or a weak effect expressed by a very low exponent value of maximum 0.2. To confirm this assumption, a set of experiments checked fuel regression rate results for chamber pressures varying from 3 to 16 atm, keeping the rest of the parameters approximately constant ($\dot{m}_{a,p} = 60$ g/s, $T_0 \cong 867$ K, and $d = 23$ mm). Chamber pressure effect was actually found to be negligible. The following correlation was obtained from the experimental results:

$$\dot{r} = 0.405 \cdot P_c^{0.035} \tag{20}$$

where $\dot{r}$ is in millimeters per second and P_c is in atmospheres. Such a minor effect is within the typical experimental spread and can practically be neglected.

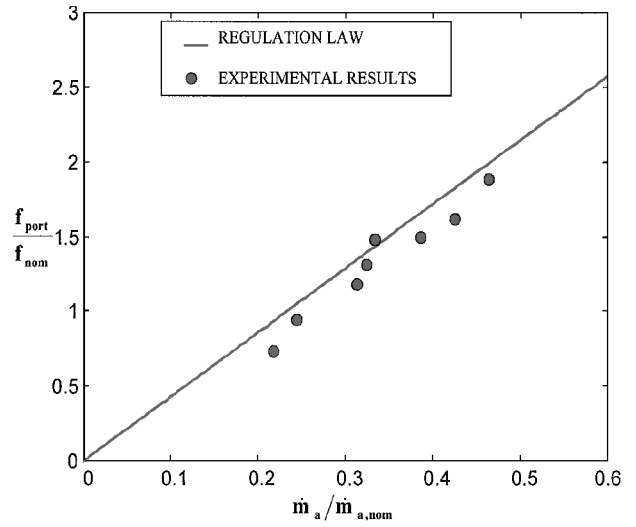

Fig. 12 Port to nominal fuel-to-air ratio as a function of the normalized overall air mass flow rate in the case of total air temperature variation, with constant port air mass flow rate and port diameter.

Port Diameter Variation

Because of the strong theoretical dependence of fuel regression rate on port diameter, it was convenient to examine experimentally the fuel regression model by varying port diameter in several series of tests, performing each series at a constant port air mass flow rate. In all tests, the air total temperature was approximately constant. The test results of port diameter variation effect were found to be incoherent with the turbulent boundary-layer theoretical model expressed by Eq. (1); hence, an empirical correlation was sought, expressing separately the individual influences of the port airflow rate and the port diameter, according to

$$\dot{r} = a\dot{m}_{a,p}^n d^q \tag{21}$$

All test data were, thus, presented together on the same graph [see Fig. 13], in terms of the regression rate related to the port air mass flow rate (characterized by the $n = 0.8$ exponent). The results indicated that $q = -0.8$, yielding the following empirical correlation:

$$\dot{r} \propto \dot{m}_{a,p}^{0.8} d^{-0.8} \tag{22}$$

This general result is of great importance because it reveals a phenomenon that deserves further examination in a separate independent study, and it is discussed in further detail subsequently. The observed behavior was encountered in several precedent works,[11,13,14] where the step between the combustor inlet and the solid fuel port was found to influence fuel regression rate.

The basic regression rate model formulated in this work [Eq. (1)] assumes the establishment of a diffusion flame within a fully developed turbulent boundary layer along the fuel grain. As a matter of

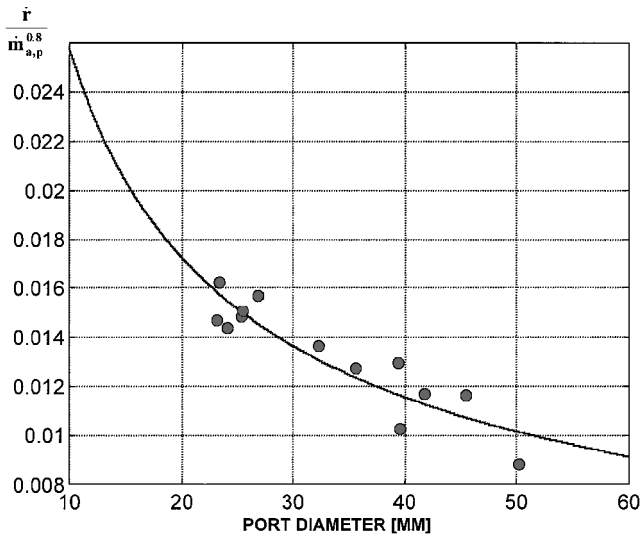

Fig. 13 Effect of port diameter on fuel regression rate for a variety of airflow rates at constant air total temperature of approximately 850 K.

fact, two regions can actually be observed in a typical SFRJ combustor: a recirculation zone where a separated flow occurs and a turbulent boundary-layer zone where the diffusion flame takes place. Zvuloni et al.[13] and Krall and Sparrow[14] demonstrated the existence of a relation between the inlet step, Reynolds number, and the heat transfer to the fuel surface in the recirculation zone. They showed that, for a given motor, the higher the inlet step is, the higher the heat transfer rate in the recirculation zone. (This effect was found to be more pronounced for lower Reynolds numbers.) In addition, it is known that the higher the inlet step is, the longer the recirculation zone. Consequently, the trend found in the present work is predictable and can be easily interpreted, by relating regression rate enhancement to the increase both of the recirculation zone and heat transfer resulting from port diameter increase in each experimental series.

The port diameter variation effect leads to the conclusion that a more comprehensive model of the fuel regression rate should be adopted, including the combustor inlet step as an additional influencing parameter. When the inlet step is expressed in terms of the port-to-inlet diameter ratio d/d_{in}, the fuel regression rate would be correlated as follows:

$$\dot{r} \propto (d/d_{\text{in}})^{s} \cdot \dot{m}_{a,p}^{n} \cdot T_0^{m} \cdot d^{-(1+n)} \tag{23}$$

When Eq. (23) is substituted in Eq. (21), and it is taken into account that in the present study the same d_{in} was applied in all of the experiments, the following equality results for these test conditions:

$$s - (1+n) = q \tag{24}$$

Applying the test values of $n = 0.8$ and $q = -0.8$ yields for the present experimental study $s = 1$, in good agreement with results found by Netzer and Gany.[11]

Corrected Regulation Law

Extending the regulation model enables the formulation of a new corrected control law for the air-division valve, incorporating the specific port diameter dependence:

$$\dot{m}_{a,p}/\dot{m}_a = (\dot{m}_{a,p}/\dot{m}_a)_{\text{nom}} \cdot (\dot{m}_a/\dot{m}_{a,\text{nom}})^{[(1-n)/n]} \cdot (d/d_{\text{nom}})^{-[(1+q)/n]} \cdot (T_0/T_{0,\text{nom}})^{-m/n} \tag{25}$$

The normalized fuel regression rate can be expressed again in its corrected form:

$$\frac{\dot{r}}{\dot{r}_{\text{nom}}} = \frac{(\dot{m}_{a,p}/\dot{m}_a)^n}{(\dot{m}_{a,p}/\dot{m}_a)_{\text{nom}}^n} \left(\frac{\dot{m}_a}{\dot{m}_{a,\text{nom}}}\right)^n \cdot \left(\frac{d}{d_{\text{nom}}}\right)^q \cdot \left(\frac{T_0}{T_{0,\text{nom}}}\right)^m \tag{26}$$

Port Diameter Variation Final Results

As in the former cases, one can simplify the general expression of the control law [Eq. (25)] for port diameter variation at approximately constant port air mass flow rate and air total temperature. In this case, the nominal conditions are defined as follows:

$$f = f_{\text{nom}} = \text{const}, \qquad \dot{m}_{a,\text{nom}} = \dot{m}_{a,\max} = 300 \text{ g/s}$$
$$T_0 = T_{0,\text{nom}} = 850 \text{ K}, \qquad (\dot{m}_{a,p}/\dot{m}_a)_{\text{nom}} = 1 \tag{27}$$

Substitution of the nominal conditions in the control law [Eq. (25)] yields a simplified expression of the port-to-total air mass flow rates ratio:

$$\dot{m}_{a,p}/\dot{m}_a = (d/d_{\text{nom}})^{-[(1+q)/n]} \cdot (\dot{m}_a/\dot{m}_{a,\text{nom}})^{[(1-n)/n]} \tag{28}$$

Making use of Eqs. (13) and (15) and substituting Eq. (15) in Eq. (28), one can obtain a useful relation between the experimental results characterized by the normalized port diameter and the respective normalized overall air mass flow rate:

$$(d/d_{\text{nom}})^{(1+q)} = C^{-n} \cdot (\dot{m}_a/\dot{m}_{a,\text{nom}}) \tag{29}$$

Substitution of Eq. (29) in the simplified regulation law [Eq. (28)] allows the hypothetical opening state of the air-division valve to be found as a function of the respective experimental normalized port diameter:

$$\dot{m}_{a,p}/\dot{m}_a = C^{(1-n)} \cdot (d/d_{\text{nom}})^{-(1+q)} \tag{30}$$

Figure 14 shows the correlation of the experimental points to hypothetical states of the air-division valve according to Eq. (30).

In addition, one can predict the fuel regression rate expected in the port diameter variation case by substituting the relevant conditions [Eq. (27)] in Eq. (26):

$$\dot{r}/\dot{r}_{\text{nom}} = C^n \cdot (d/d_{\text{nom}})^q = C^{[n/(1+q)]} \cdot (\dot{m}_a/\dot{m}_{a,\text{nom}})^{[q/(1+q)]} \tag{31}$$

The theoretical and experimental normalized fuel regression rates are shown in Fig. 15, as a function of the normalized total air mass flow rate, revealing a very good agreement.

As shown in the other cases, the fuel-to-air ratio depends on the port-to-total air mass flow rates ratio [see Eqs. (11) and (19)]. Substitution of the port-to-total air mass flow rates ratio, relevant to the actual port diameter variation case [Eq. (30)], in the fuel-to-air ratio expression, leads to the following normalized fuel-to-air ratio:

$$f_p/f_{\text{nom}} = C^{-1} \cdot (\dot{m}_a/\dot{m}_{a,\text{nom}}) = C^{(n-1)} \cdot (d/d_{\text{nom}})^{(1+q)} \tag{32}$$

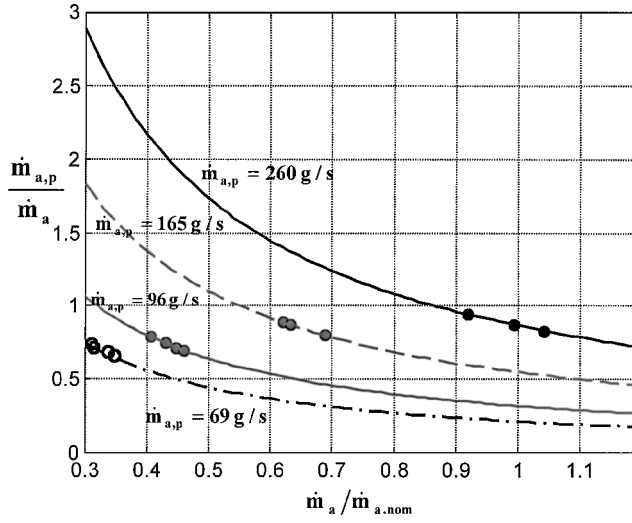

Fig. 14 Correlation of the experimental points to hypothetical opening states of the air-division valve as a function of the normalized overall air mass flow rate, for fuel port diameter variation at constant total air temperature, for several constant port air mass flow rate cases.

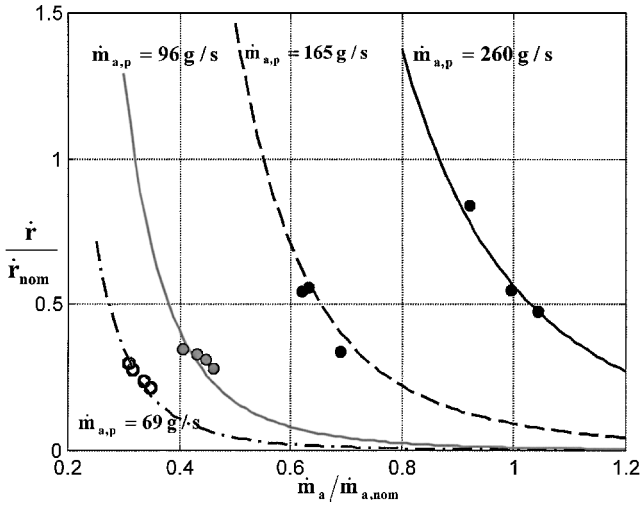

Fig. 15 Normalized fuel regression rate (experimental and theoretical) as a function of normalized overall air mass flow rate, for fuel port diameter variation at constant total air temperature, for several constant port air mass flow rate cases.

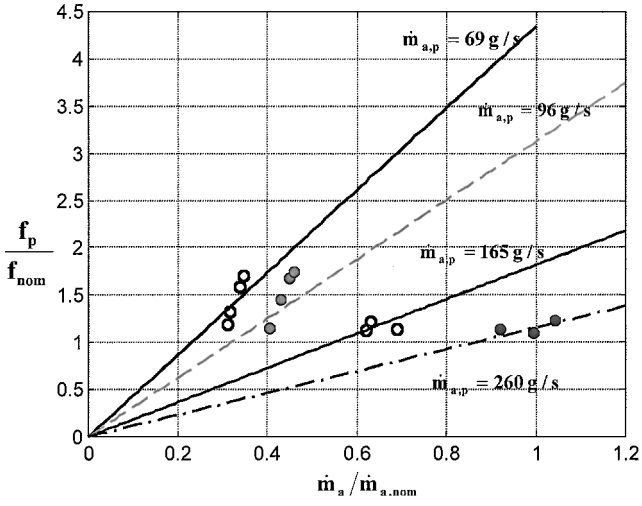

Fig. 16 Port to nominal fuel/air ratio as a function of normalized overall air mass flow rate, for fuel port diameter variation at constant total air temperature, for several constant port air mass flow rate cases.

Figure 16 shows the theoretical and experimental normalized port fuel-to-air ratio as a function of the normalized overall air mass flow rate. A good agreement can be observed between the theoretical prediction and the experimental results. Nevertheless, note that the testing of port diameter influence is based on a limited number of experiments, due to the physical limitations of the fuel grain. Therefore, the normalized overall air mass flow rate ranges corresponding to each of the constant port air mass flow rate series are relatively narrow and do not represent the full regulation capability.

Finally, by substituting the test results of the individual effects in the general regulation law [Eq. (25)], one obtains an experimentally backed expression of the air-division valve control law:

$$\dot{m}_{a,p}/\dot{m}_a = (\dot{m}_{a,p}/\dot{m}_a)_{\text{nom}} \cdot (\dot{m}_a/\dot{m}_{a,\text{nom}})^{0.25} \cdot (d/d_{\text{nom}})^{-0.25} \cdot (T_0/T_{0,\text{nom}})^{-1.25} \quad (33)$$

This expression consists of the individual power law correlations of major influencing parameters: $n = 0.8$ for air mass flow rate effect (in agreement with the theory of convective heat transfer in turbulent boundary layer), $m = 1$ for total air temperature effect, $q = -0.8$ for the port diameter effect, and practically no effect of chamber pressure.

Conclusions

The present study provides a comprehensive understanding and characterization of SFRJ regulation by a controlled division of the overall incoming airflow to combustor-port and bypass flows, accomplished by an air-division valve. Analysis of the concept has yielded the formulation of a general regulation law, determining the opening state of the air-division valve at any point over a wide envelope of altitudes and Mach numbers and, hence, ensuring, for instance, motor operation at a constant desirable fuel-to-air ratio.

An experimental examination of the theoretical approach enabled the comparison of the theoretical prediction to practical results by isolating key parameters influencing the fuel regression rate, such as port air mass flow rate, total air temperature, port diameter, and pressure, and testing their individual effects one at a time. The experimental results covered all major aspects relevant to SFRJ combustor operation, demonstrating the characteristics over wide operating ranges and revealing very good agreement with the theoretically predicted values. A composition of the individual effects yielded a comprehensive regulation law based on test data and backed by theoretical considerations.

The study has demonstrated the feasibility and effectiveness of the air-division valve concept for regulating SFRJ operation over a broad flight envelope, experimentally simulating flight altitudes from sea level to 13 km and flight Mach numbers from 1.5 to 4.7.

Acknowledgments

The support of Gutwirth Scholarship and Asher Peled Fundations is greatly acknowledged.

References

[1]Pelosi-Pinhas, D., and Gany, A., "Solid-Fuel Ramjet Regulation by Means of an Air-Division Valve," *Journal of Propulsion and Power*, Vol. 16, No. 6, 2000, pp. 1069–1074.

[2]Timnat, Y. M., "Recent Developments in Ramjets, Ducted Rockets and Scramjets," *Progress in Aerospace Sciences*, Vol. 27, No. 3, 1990, pp. 201–235.

[3]"Solid Fuel Ramjet," United Technologies Chemical Systems, San Jose, CA, 1980, pp. 12–14.

[4]Leisch, S., and Netzer, D. W., "Solid Fuel Ramjets," *Tactical Missile Propulsion*, edited by G. E. Jensen and D. W. Netzer, Vol. 170, Progress in Astronautics and Aeronautics, AIAA, Reston, VA, 1996, Chap. 13, pp. 469–496.

[5]Krishnan, S., and George, P., "Solid Fuel Ramjet Combustor Design," *Progress in Aerospace Sciences*, Vol. 34, No. 4, 1998, pp. 219–256.

[6]Krishnan, S., George, P., and Sathyan, S., "Design and Control of Solid-Fuel Ramjet for Pseudovacuum Trajectories," *Journal of Propulsion and Power*, Vol. 16, No. 5, 2000, pp. 815–822.

[7]Keirsey, J. L., "Solid Fuel Ramjet Flow Control Device," U.S. Patent 628,688, filed 1986.

[8]Hadar, I., and Gany, A., "Fuel Regression Rate Mechanism in a Solid Fuel Ramjet," *Propellants, Explosives, Pyrotechnics*, Vol. 17, No. 3, 1992, pp. 70–76.

[9]Cohen-Zur, A., and Natan, B., "Experimental Investigation of a Supersonic Combustion Solid Fuel Ramjet," *Journal of Propulsion and Power*, Vol. 14, No. 6, 1998, pp. 880–889.

[10]Cruise, D. R., "Theoretical Computation of Equilibrium Composition, Thermodynamic Properties, and Performance Characteristics of Propellant Systems (PEP code)," Naval Weapons Center, China Lake, CA, April 1979.

[11]Netzer, A., and Gany, A., "Burning and Flameholding Characteristics of a Miniature Solid Fuel Ramjet Combustor," *Journal of Propulsion and Power*, Vol. 7, No. 3, 1991, pp. 357–363.

[12]Rosner, D. E., *Transport Processes in Chemically Reacting Flow Systems*, Dover, Mineola, NY, 2000, Chap. 5, pp. 215–285.

[13]Zvuloni, R., Levy, Y., and Gany, A., "Investigation of a Small Solid Fuel Ramjet Combustor," *Journal of Propulsion and Power*, Vol. 5, No. 3, 1989, pp. 269–275.

[14]Krall, K. M., and Sparrow, E. M., "Turbulent Heat Transfer in the Separated, Reattached and Redevelopment Regions of a Circular Tube," *Journal of Heat Transfer*, Vol. 88, No. 1, 1966, pp. 131–136.